# Laminar burning velocity measurements and stability map determination of Fe-$N_2/O_2$ mixtures in a tube burner

M. Fedoryk*[1], B. Stelzner[1], S. Harth[1], D. Trimis[1]

[1]GERMANY, Karlsruhe Institute of Technology, Engler-Bunte Institute, Division of Combustion Technology

**Abstract**

This study presents the experimental investigation of laminar burning velocity of iron dust in different nitrogen-oxygen mixtures using a tube burner. The laminar burning velocity was calculated based on the shape of the flame front captured by a camera. Results showed that an increase in oxygen concentration increased the laminar burning velocity of iron dust. The study also presents preliminary results of the investigation of the influence of particle diameter on the combustion process.

## Introduction

The circular economy concept is gaining popularity due to the need for resilient and sustainable supply chains. Circular fuels are seen as an attractive alternative to fossil fuels in many countries, especially when the latter ones have to be imported. For such an application, seasonal energy storage should be possible for year-round power generation. Efforts are being made to integrate novel fuels into the existing electricity generation systems. Metal powders are being studied for carbon-free energy cycle systems, with iron being one of the most promising fuels [1].

Combustion of iron powder has gained much interest in last years, as iron is seen to be able to play a role of a carbon-free energy carrier in a closed loop, where the iron oxide is reduced to elemental iron by thermochemical and electrochemical means in the storage part of the cycle. During power generation, the iron powder is burnt, releasing heat that can be converted into electricity. The iron oxide formed in this way can be later reduced directly in an electrochemical way or using hydrogen.

Iron and iron oxide powder are safe and easy to store and transport, allowing the oxidation and reduction sites to be located far apart. Coal-fired power plants can be retrofitted to iron powder firing operation, reducing the capital expenditures of introducing the proposed technology and utilizing the experience of the workforce for the modified operation of thermal power plants.

During the combustion process, iron and iron oxides remain mostly in a solid or liquid phase. However, nanoparticle clouds formed from condensing iron and iron oxides around the burning particle have been observed [2] [3] [4]. The nonvolatile particles usually react heterogeneously with air, but an increase in oxygen content and initial temperature of the reactants can switch the combustion regime to a hybrid homogeneous-heterogeneous type. It has been demonstrated that in a single iron particle burner, iron particles can burn heterogeneously and the resulting particles are similar to the raw iron particles used [5].

## Experimental set up

Different burner constructions and operating conditions have been used to investigate metal powder combustion since the late 1980s, including Bunsen-type burners, Hartmann tubes, and counter-flow reactors. The flame propagation in iron powder burners has also been investigated under reduced gravity, and the influence of supporting fuels such as methane has been of interest in recent years.

In this study, a metal powder seeder of air knife type introduced by Goroshin et al. was applied [6]. The scheme of the investigation set up is shown in Fig 1.

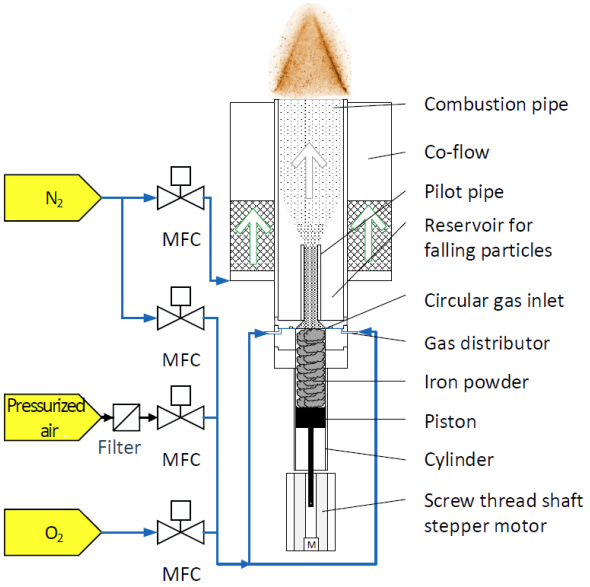


**Figure 1:** Scheme of the experimental test rig.

The iron powder used for combustion is contained in a tube in the bottom part and is moved upwards by a piston connected to a stepper motor through a threaded shaft. The powder is dispersed in an area of a circular horizontal gap, which is approximately 30 µm high, and where high gas velocity is generated. The air mass flow in the seeder/burner and in the co-

* Corresponding author: michal.fedoryk@kit.edu

flow stream is controlled by mass flow controllers (MFC) on the feed lines. Once the powder suspension passes through the slit area, it goes through a 45° constriction and a pilot tube before entering the combustion tube with a 20.5 mm inner diameter ($R_0$ = 10.25 mm). This shape of the tube prevents the powder from forming a columnar structure over the air inlet due to the adhesion forces. The narrowing section was placed after the air slit and a pilot pipe with a smaller diameter was introduced based on observations during preliminary tests with optical access to the seeder outlet.

The required low air velocities promote agglomeration of metal dust on the combustion tube inner walls. As the iron powder suspension exits the pilot tube, the flow slows down and the particles tend to stick to the wall of the larger tube. The design of the burner setup includes two concentric tubes for the seeded flow to minimize seeding fluctuations related to the detachment of residues from the walls. The inner tube is the pilot tube with a length of 10 cm, and the outer one is the combustion tube with a length of 35 cm downstream from the pilot tube outlet.

The falling powder is collected in a separate container. The length of the pilot tube was adjusted to ensure there is sufficient free space for the falling powder and to minimize the influence of this avalanche-like event on the conditions in the reaction zone.

The particle mass flow at the burner outlet is calculated based on the powder supplied by the flask and the quantity remaining in the separate container. To increase flame stability at the burner rim and prevent external influences on the flame, the outlet tube is surrounded by a co-flow with a 58.8 mm diameter. In the experiments presented in the paper, the co-flow stream was fed with nitrogen whose velocity corresponded to the mean outlet velocity at the burner. In the latter part, in which the combustion of the blends of iron powder is investigated, atmospheric air was used in co-flow. All gases were supplied to the burner at ambient temperature.

**Iron powder**

Two types of iron powder were used in the experiments. Both of them were carbonyl iron powder, as the particles are supposed to be of spherical shape [7]. The finer one (powder A) was supplied by Carl Roth GmbH, Karlsruhe, Germany (art. № 3718, Fe > 99.5%) and the one with larger particles (powder B) by Eckart GmbH, Hartenstein, Germany (<32 µm, Fe>99.8%). The particle size distribution of both powders were measured using a dry dispersion unit RODOS and a compact laser diffraction sensor HELOS (H0309), Sympatec GmbH, Clausthal-Zellerfeld, Germany.

As can be seen in the particle size distribution shown in Fig. 2, the half of the total iron mass was provided by particles smaller than 6.2 µm in case of powder A and 16.3 µm for powder B.

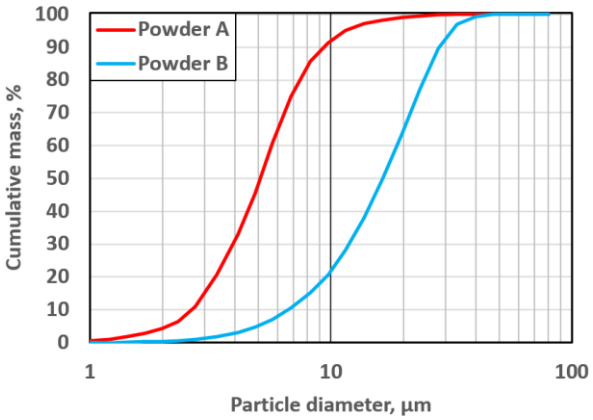


**Figure 2:** Cumulative particle size distribution of both powders.

**Laminar burning velocity**

The laminar burning velocity can be estimate in a pipe burner by measurement of the outlet velocity profile and determination of the flame surface shape. If the stream of the educts leaves the burner in a laminar regime, a simply mass balance can be drawn. The product of the tube cross section area $A_{T,0}$ and axial velocity of the gas $u_0$ should be equal to the product of the flame front area $A_F$ and the laminar burning velocity $s_L$:

$$A_{T,0} \cdot u_0 = A_F \cdot s_L$$

By conversion of the equation above, the laminar burning velocity is equal to:

$$s_L = \frac{A_{T,0}}{A_F} \cdot u_0$$

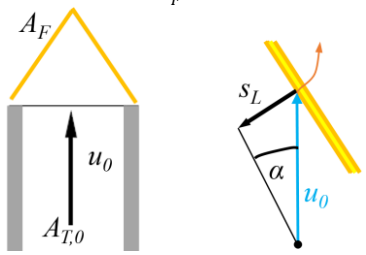


**Figure 3:** Laminar burning velocity determination.

As the flow is laminar, the flow layers do not mix, and the balance is valid for every annulus of the flow. Taking this into account, the ratio of the tube cross-sectional area to the flame front area $A_{T,0}/A_F$ can be estimated geometrically with the sine between the flame front and the longitudal axis of the burner $sin\alpha$.

In the performed experiments, laminar burning velocity was calculated based on two measured values: the local initial axial velocity $u_0(r)$ and flame inclination $sin\ \alpha(r)$ using the following formula:

$$s_L(r) = u_0(r) \cdot sin\ \alpha(r)$$

Two regions are sensitive to the external forces as well as internal flame influence. Around of the flame tip, the increase of the heat transfer via convection and, especially in the case of combusted particles – radiation can be observed. This leads to the increase of the measured burning velocity that no longer corresponds to the unaffected laminar conditions. Taking this into

account, the two one-third of the radius regions beginning on r=0 and r=$R_0$ were excluded and the laminar burning velocity was determined in the region $^1/_3 < r/R_0 < {}^2/_3$.

The axial velocity of the particles $u_0(r)$, was determined in the PIV measurements performed in this burner previously and described in [8]. As the particle size distribution and the operating conditions in the earlier experiments were similar, it was assumed that the assumption of the same axial velocity profile is valid.

**Flame imaging**

The flame imaging was performed at 8 Hz using a 12-bit gray scale mvBlueFOX camera (Matrix Vision GmbH, Oppenweiler, Germany) with a resolution of 1360×1024 pixels. A band-pass filter of 450±10 nm was placed in front of the lens to reduce noise.

The images were taken for at least 30 seconds. The images captured in this period were then averaged. Subsequently, to achieve a cross-sectional image of the flame front over the averaged time, the Abel transformation was performed [9]. An example is shown in Fig. 4.

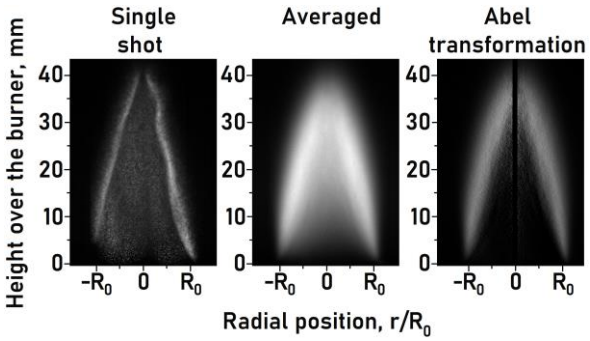


**Figure 4:** Image processing, 19% $O_2$ in the gas phase, average inlet velocity 40 cm/s.

In the averaged image, an unsteady behavior of the flame can be observed in the averaged photo, especially in the upper part of the flame, which does not create a sharp tip. It can be seen also after Abel transformation, where the luminous region does not create a thin line. On the other hand, the recorded reaction zone is usually significantly larger in the metal dust flames than in gas flames. This is caused by the fact that the particles also emit light through thermal radiation after the chemical reaction [5], but due to their size, they need more time to cool down compared to, for example, soot particles. In fact, the high luminosity of particles also affects the correct determination of the flame front after the combustion process. Due to the significant temperature variations throughout combustion process, some images may be partially saturated in high-temperature regions and, at the same time, some colder particles may not be detected at all in the same image [10].

**Measurement results and discussion**

In all experiments, the same stoichiometric mixture, based on $Fe_2O_3$, was applied. There, in order to keep the fuel-air equivalence ratio $\Phi = 1.0$, the particle number density must increase with the increased oxygen concentration in the gas phase.

Preliminary experiments, in which different oxygen concentrations in the gas phase were applied, showed different behavior of the flames obtained.

The higher oxygen content leads to an increased flame temperature and thus to a more intense Planck radiation from the particles (Fig. 5). It turned out to be impossible, to perform all the experiments with the same outlet velocity. While a reduced $O_2$ concentration led to flame lifting and extinction, the oxygen enrichment of the gas phase led to increased flame stability. Because of this phenomenon, it was decided to perform experiments with several outlet velocities of the iron suspension. This should be valid, as it was previously demonstrated that around the fuel-air equivalence ratio $\Phi = 1$, the burning velocity is independent of the outlet velocity from the tube [8].

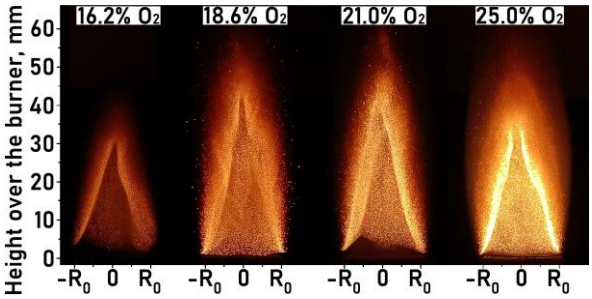


**Figure 5:** Single shots of iron flames ($\Phi = 1$) at 16.2%, 18.6%, 21.0% and 25% $O_2$ in the gas phase taken with ISO 100 and $^1/_{8000}$ s.

The measurements were performed under the operating conditions shown in Tab. 1. The oxygen content in the gas phase was varied from 17 to 25 vol-%. In order to keep the air to fuel equivalence ratio equal to unity in respect to $Fe_2O_3$, the particle concentration was accordingly varied from 520 to 760 g/m³. The average inlet velocity of the educts $u_{0,avg}$ was chosen based on the preliminary experiments in order to achieve stationary iron flames. The inlet temperature was equal to 25°C.

**Table 1:** Operating conditions of the investigated cases.

| | *1* | *2* | *3* | *4* | *5* |
|---|---|---|---|---|---|
| $O_2$ conc. (vol-%) | 17 | 19 | 21 | 23 | 25 |
| $N_2$ conc. (vol-%) | 83 | 81 | 79 | 77 | 75 |
| part. conc. (g/m$^3$) | 520 | 580 | 640 | 700 | 760 |
| $u_{0,\,avg}$ (cm/s) | 30 | 40 | 45 | 45 | 45 |

The procedure described in the previous chapters was used to calculate the laminar burning velocity. The laminar burning velocity of the iron suspensions investigated is between 10 and 30 cm/s (Fig. 6). In the case of air combustion (i.e. 21% $O_2$), the result is

slightly lower than reported by Tang et al. with the corresponding iron particles diameter [11]. An increase of oxygen concentration leads to an increase of the laminar burning velocity of the iron dust. The similar dependence were observed by Goroshin and Julien for stoichiometric and fuel-rich aluminum powder combustion [6], [12], [13] and by Tang for iron combustion in $O_2$/He and $O_2$/Xe mixtures [14].

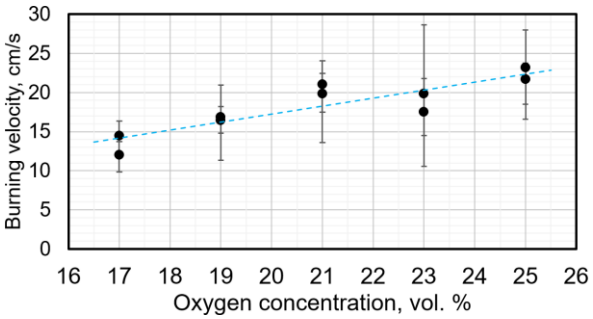


**Figure 6:** Measured burning velocity of iron dust flames of powder A (points) and linear approximation (blue dashed line).

While performing the experiments with the nitrogen in the co-flow, it was observed that the detachment of the flame from the edge of the exit pipe was more frequent in comparison to the previous application of air in this stream in this burner described in [8].

**Particle size and flame stability**

In the second part, the influence of the particle size on the flame behavior was investigated. For this reason, three powders were combusted in the atmospheric air under the same operating conditions: $u_{0,avg}$ = 40 cm/s and Φ = 1.0. Atmospheric air was supplied in the co-flow. The ratios of powder A to powder B were equal to 100:0, 75:25 and 50:50 (mass). The powder B does not create a stationary flame front under mentioned conditions.

It was observed that all the blends could be combusted in lasting flames. In all cases, a conical flame front was detected (Fig. 7). When using only powder A, there were few particles leaving the luminous zone and emit visible light several millimeters downstream. As the coarser fraction was added, a number of hot particles can be seen downstream to the flame front. First, because of their greater mass and inertia, particles require more time to heat up and reach the temperature of thermal runaway [15]. For the same reason, the combustion and cooling process last longer in comparison to smaller particles. Once ignited in the region of the flame front, which consists of the smaller particles, the larger ones tend to burn downstream in a single particle mode.

However, the higher proportion of the coarser fraction, the more sensitive the flame front. This manifested itself in more frequent detachment of the reaction zone from the burner rim. The conical flame front is slightly less intensive in 50:50 blend in comparison to slammer particles. However, if one assuming that it is mainly the powder A, the stabilizing effect of the coarser fraction during combustion can be observed. Namely, it was not possible to stabilize flame consisting only of powder A at Φ = 0.5, so as if the coarser fraction would not exist in the discussed case.

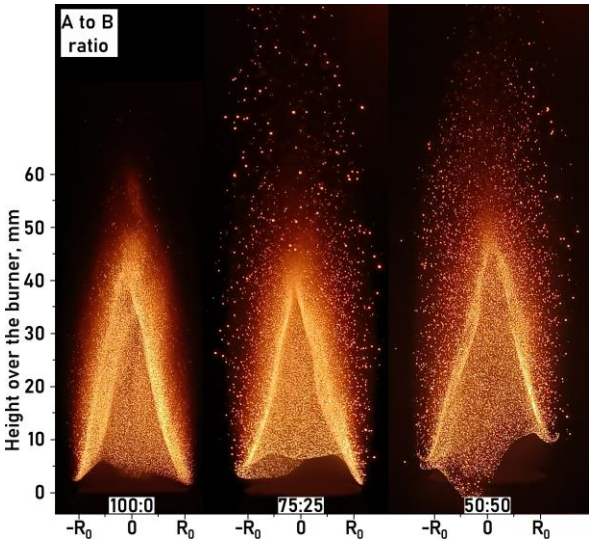


**Figure 7:** Snapshots of iron flames (Φ = 1) of following powders: CR/E: 100:0 (left), 75:25 (center), 50:50 (right). RGB camera above and grayscale at the bottom.

**Acknowledgements**

The present research work contributes to the MTET program, Resource and Energy Efficiency, Anthropogenic Carbon Cycle (38.05.01) of Helmholtz Association. This work was performed within the cluster project Clean Circles. Financial support by the Strategy Founds of the KIT Presidium is gratefully acknowledged. Special thanks for M. Deutschmann und K. Hirsch for the measurements of the particle size distribution of the iron powder.

**References**

[1] J. M. Bergthorson, "Recyclable metal fuels for clean and compact zero-carbon power," *Progress in Energy and Combustion Science*, no. 68, pp. 169-196, 18 June 2018.

[2] H. Wiinikka, T. Vikström, J. Wennerbo, P. Toth and A. Sepman, "Pulverized Sponge Iron, a Zero-Carbon and Clean Substitute for Fossil Coal in Energy Applications," *Energy Fuels*, pp. 9982-9989, 16 08 2018.

[3] D. Ning, Y. L. Shoshin, J. A. van Oijen, G. Finotello and L. P. H. de Goey, "Critical temperature for nanoparticle cloud formation during combustion of single micron-sized iron particle," *Combustion and Flame*, pp. 1-8, 12 07 2022.

[4] T. Li, F. Reinauer, B. Böhm and A. Dreizler, "Visualizing particle melting and nanoparticle formation during single iron particle oxidation

with multi-parameter optical diagnostics," *Combustion and Flame,* pp. 1-15, 11 2022.

[5] D. Ning, Y. Shoshin, J. A. van Oijen, G. Finotello and L. P. H. de Goey, "Burn time and combustion regime of laser-ignited single iron particle," *Combustion and Flame,* no. 230, pp. 1-10, 15 3 2021.

[6] S. Goroshin, M. Bidabadi and J. H. S. Lee, "Quenching Distance of Laminar Flame in Aluminum Dust Clouds," *Combustion and Flame,* no. 105, pp. 147-160, 1 4 1996.

[7] D. Bloemacher, "Carbonyl iron powders: Its production and new developments," *Metal Powder Report,* vol. 45, no. 2, pp. 117-119, 1990.

[8] M. Fedoryk, B. Stelzner, S. Harth and D. Trimis, "Experimental investigation of the laminar burning velocity of iron-air flames in a tube burner," *Applications in Energy and Combustion Science,* no. 13, pp. 1-6, March 2023.

[9] V. Dribinski, A. Ossadtchi, V. A. Mandelshtam and H. Reisler, "Reconstruction of Abel-transformable images: The Gaussian basis-set expansion Abel transform method," *Review of Scientific Instruments,* vol. 7, no. 73, pp. 2634-2642, 21 June 2002.

[10] D. Ning, Y. Shoshin, M. van Stiphout, J. van Oijen, G. Finotello and P. de Goey, "Temperature and phase transitions of laser-ignited single iron particle," *Combustion and flame,* no. 236, pp. 1-11, 2022.

[11] F.-D. Tang, S. Goroshin, A. Higgins and J. Lee, "Flame propagation and quenching in iron dust clouds," *Proceedings of the Combustion Institute,* vol. 2, no. 32, pp. 1905-1912, 2009.

[12] S. Goroshin, J. Palečka and J. M. Bergthorson, "Some fundamental aspects of laminar flames in nonvolatile solid fuel suspensions," *Progress in Energy and Combustion Science,* no. 91, pp. 1-57, 1 2 2022.

[13] P. Julien, J. Vickery, S. Goroshin, D. Frost and J. Bergthorson, "Freely-propagating flames in aluminum dust clouds," *Combustion and Flame,* vol. 162, no. 11, pp. 4241-4253, 2015.

[14] F.-D. Tang, S. Goroshin and S. Higgins, "Propagation regime of iron dust flames," NASA Technical Reports Server, 2012.

[15] X. Mi, A. Fujinawa and M. Bergthorson, "A quantitative analysis of the ignition characteristics of fine iron particles," *Combustion and Flame,* no. 240, pp. 1-17, 2022.